Available online at www.sciencedirect.com
SCIENCE DIRECT®
International Journal of Thermal Sciences 45 (2006) 870–881
International Journal of Thermal Sciences
www.elsevier.com/locate/ijts

Slip-flow and heat transfer in rectangular microchannels with constant wall temperature ☆

M. Renksizbulut *, H. Niazmand, G. Tercan

University of Waterloo, Mechanical Engineering Department, Waterloo, ON, Canada N2L 3G1

Received 10 September 2005; accepted 8 December 2005

Available online 3 February 2006

Abstract

Rarefied gas flow and heat transfer in the entrance region of rectangular microchannels are investigated numerically in the slip-flow regime. A control-volume based numerical method is used to solve the Navier–Stokes and energy equations with velocity-slip and temperature-jump conditions at the walls. The effects of Reynolds number ($0.1 \leqslant Re \leqslant 10$), channel aspect ratio ($0 \leqslant \alpha^* \leqslant 1$), and Knudsen number ($Kn \leqslant 0.1$) on the simultaneously developing velocity and temperature fields, and on the key flow parameters like the entrance length, the friction coefficient, and Nusselt number are examined in detail. In the entrance region, very large reductions are observed in the friction factor and Nusselt number due to rarefaction effects, which also extend to the fully developed region (though at much lower levels). Current results show that the friction and heat transfer coefficients are less sensitive to rarefaction effects in corner-dominated flows as in square channels when compared to flows between parallel plates. Practical engineering correlations are proposed for the friction and heat transfer coefficients in rectangular and trapezoidal channels.

Keywords: Slip-flow; Rarefaction; Rectangular microchannel; Entrance region; Friction coefficient; Temperature-jump; Heat transfer coefficient; Trapezoidal channel

1. Introduction

An important effect associated with gas flows in microchannels, where the typical length scales are measured in microns, is the rarefaction effect. Rarefaction can occur at low-pressure gas flows or in microchannels at normal pressures. The Knudsen number is a measure of the degree of rarefaction, which is defined as the ratio of the mean free path to the appropriate macroscopic length scale of the flow. For Knudsen numbers in the range $10^{-3} \leqslant Kn \leqslant 10^{-1}$, deviations from continuum behavior arise near the walls where, in a thin layer called the Knudsen layer, molecular collisions with the walls dominate over intermolecular collisions. It is well established that for this range of Knudsen numbers (slip-flow regime), the standard Navier–Stokes and energy equations can still be used with modifications to the boundary conditions allowing for velocity-slip and temperature-jump at the walls.

The behavior of rarefied gas flows in macrochannels have been studied in connection with aerospace engineering and vacuum technology, where a clear understanding of the properties of rarefied gas flows is important [1]. Recent advances in micro and nano-fabrication technologies have opened a new area where the dynamics of rarefied gas flows are applicable as well. Gas flows under standard condition where the molecular mean free path λ is typically 70 nm are often encountered in microchannels. Considering the typical hydraulic diameters of such channels (1 to 100 μm), the associated Knudsen numbers indicate some level of rarefaction even at normal pressures.

Gas flows in microchannels have received considerable attention and have been studied experimentally, numerically and analytically; e.g., Wu and Little [2], Pfahler et al. [3], Beskok and Karniadakis [4], Arkilic et al. [5,6], Harley et al. [7], Morini and Spiga [8], Beskok [9], Meinhart et al. [10], Jang and Were-

☆ A preliminary version of this paper was presented at ICMM2005: Third International Conference on Microchannels and Minichannels, held at University of Toronto, June 13–15, 2005, organized by S.G. Kandlikar and M. Kawaji, CD-ROM Proceedings, ISBN: 0-7918-3758-0, ASME, New York.

* Corresponding author. Tel.: (+519) 884 9674 ext 3977; fax: (+519) 885 5862.

E-mail address: metin@uwaterloo.ca (M. Renksizbulut).

1290-0729/$ – see front matter
doi:10.1016/j.ijthermalsci.2005.12.008

Nomenclature

$2a$	longer side of the channel
$2b$	shorter side of the channel
C_f	friction coefficient, $\tau_w/(\rho U_i^2/2)$
c_p	specific heat at constant pressure
D_h	hydraulic diameter, $4ab/(a+b)$
h	heat transfer coefficient
k	thermal conductivity
Kn	Knudsen number, λ/D_h
Nu	Nusselt number, hD_h/k
p	pressure
Pr	Prandtl number, $c_p\mu/k$
$\Re$	specific gas constant
Re	Reynolds number, $\rho U_i D_h/\mu$
T	temperature
u, v, w	velocity components in the x, y, z directions
U_i	uniform inlet velocity
$\vec{V}$	velocity vector
x^+	non-dimensional axial position, $x/(D_h Re)$
x^*	reciprocal Graetz number, $x/(D_h Re\, Pr)$

Greek symbols

α^*	aspect ratio, b/a
λ	molecular mean-free-path
τ_w	wall shear stress, $\mu(\partial u/\partial n)_w$
ρ	density
μ	dynamic viscosity

Subscripts

fd	fully developed
i	inlet
w	wall
m	bulk mean

ley [11], Xue and Fan [12], Araki et al. [13], Hsieh et al. [14], Turner et al. [15], Colin [16], Morini et al. [17], among others. The experimental data from these studies strongly support the applicability of the continuum approach in combination with slip boundary conditions to model the flow and heat transfer problems in microchannel flows with relatively low rarefaction effects. Otherwise, numerical results show significant deviation from experimental data. Compressibility effects on friction factor and the application of higher order slip conditions were also investigated. Most of the numerical simulations and analytical solutions were performed in 2-D Cartesian coordinates often with simplifying assumptions in the governing equations. A survey of the available literature on low Mach number flows indicates a shortage of information for 3-D flows in the slip regime, such as in short microchannels where the entrance region may play an important role.

Slip-flow heat transfer in microchannels has also been studied by several researchers; e.g., Inman [18], Barron et al. [19,20], Kavehpour et al. [21], Ameel et al. [22], Larrodé et al. [23], Yu and Ameel [24,25], Tunc and Bayazitoglu [26], Hadjiconstantinou and Simek [27], Asako [28], among others. It is found that the temperature-jump effect is very important and should be included in the modeling of the slip-flow heat transfer problems, and neglecting this effect leads to a significant over prediction of heat transfer rate. Moreover, it is found that when both velocity-slip and temperature-jump conditions are taken into account, Nusselt number decreases monotonically with increasing Knudsen number in the full-accommodation cases. Tunc and Bayazitoglu [26] performed an analytical study of convective heat transfer in an isoflux rectangular microchannel. The flow field was assumed to be fully developed both thermally and hydrodynamically, and the heat transfer rates were given for a wide range of aspect ratios and several Pr numbers. Under the same flow conditions, Hadjiconstantinou and Simek [27] studied the constant wall temperature problem in 2-D micro and nano-channels in the slip and transitional flow regimes. The effect of axial conduction was also included and it was found that this effect increases the Nusselt number in microchannel flows.

Studies on thermally developing micro flows in the literature are limited to the application of fully developed analytical slip velocity profiles in the solution of the energy equation. Larrodé et al. [23] provided an analytical solution for developing heat transfer in a constant wall temperature circular tube, where the fully developed slip velocity profile was employed. The temperature-jump condition was applied at the wall in the slip-flow regime. Yu and Ameel [24,25] presented an analytical treatment of the slip-flow problem for rectangular microchannels. Developing and fully developed Nusselt numbers were obtained for hydrodynamically fully developed slip-flow. Note that in these studies, the effects of axial heat conduction, which become important for low Peclet number ($Pe = Re\, Pr$) conditions typical of microchannel gas flows were neglected.

In the present work, incompressible gas flows and heat transfer in rectangular microchannels of various aspect ratios have been investigated for Knudsen numbers related to the slip-flow regime. Three-dimensional Navier–Stokes and energy equations with velocity-slip and temperature-jump boundary conditions have been solved numerically by a control-volume method. Axial molecular diffusion of the momentum and heat are also included in the analysis. In particular the entrance region has been investigated, where the major pressure drop and heat transfer occur in short channels that are frequently encountered in modern compact heat exchangers as well as in various types of micro-fluidic devices found in MEMS.

2. Formulation

The coordinate system located at the center of the channel and the basic geometric variables are shown in Fig. 1. The aspect ratio is given by $\alpha^* = 2b/2a$, where $2b$ denotes the shorter side of the channel. The principal flow is in the x-direction. The

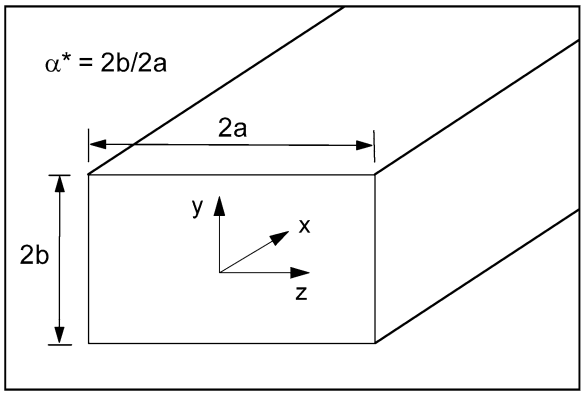

Fig. 1. Channel geometry and the coordinate system.

laminar, constant-property, viscous flow under study is governed by the usual continuity, momentum and energy equations as follows:

$$\vec{\nabla}\cdot\vec{V}=0 \tag{1}$$

$$\rho\frac{D\vec{V}}{Dt}=-\nabla p+\mu\nabla^2\vec{V} \tag{2}$$

$$\rho c_p\frac{DT}{Dt}=k\nabla^2 T \tag{3}$$

Note that body forces and viscous dissipation are ignored in the present work. The prescribed inflow boundary conditions correspond to uniform flat profiles such that $u=U_i=U_m$, $v=w=0$, and $T=T_i$, where subscripts i and m refer to inlet and bulk mean conditions, respectively. For outflow, zero-gradients along the axial flow direction are applied; that is $\partial f/\partial x=0$, where $f=u,v,w,T$. Since the problem under study is taken as a mass-driven flow, the pressure is set equal to zero at the outlet, while zero pressure gradients are assigned at all other boundaries including the inlet. The channel walls are uniformly at T_w, while the flow satisfies the velocity-slip and temperature-jump conditions at the walls. According to slip-flow theory, the gas velocity at the wall is different from the wall velocity in proportion to the local velocity gradient normal to the wall. Maxwell [29] derived the first order slip velocity for a dilute monatomic ideal gas as:

$$u-u_w=\alpha\left(\frac{2-\sigma_v}{\sigma_v}\right)\lambda\left(\frac{\partial u}{\partial n}\right)_w+\frac{3}{4}\frac{\mu}{\rho T_w}\left(\frac{\partial T}{\partial s}\right)_w \tag{4a}$$

The other velocity components are specified similarly. Here, the subscript w identifies a wall with normal coordinate n and tangential coordinate s. Similarly, the gas temperature at the wall differs form the wall temperature in proportion to the local normal temperature gradient. The corresponding temperature-jump condition was derived by von Smoluchowski [30] as:

$$T-T_w=\beta\left(\frac{2-\sigma_T}{\sigma_T}\right)\left(\frac{2\gamma}{\gamma+1}\right)\frac{\lambda}{Pr}\left(\frac{\partial T}{\partial n}\right)_w+\frac{u^2}{4\Re} \tag{4b}$$

The velocity-slip condition (Eq. (4a)) contains the tangential-momentum accommodation coefficient σ_v which is equal to zero for specular molecular reflections at a wall, whereas a totally diffuse reflection corresponds to $\sigma_v=1$ [31]. Similarly, σ_T in Eq. (4b) is the energy accommodation coefficient, which is equal to 1 if the molecule acquires the wall temperature upon collision, and equal to zero if it retains its original temperature. For a given gas, the accommodation coefficients σ_v and σ_T depend on the surface finish and the fluid temperature and pressure, and are normally determined experimentally. In typical engineering applications, σ_T is close to 0.9 [22]. Considering the approximate nature of the slip boundary conditions, they are taken as unity in the present study. The other coefficients α and β introduce corrections to account for the approximate nature of the original derivations of Maxwell and von Smoluchowski [32]. For air, α and β are usually taken to be equal to unity [31].

According to Kennard [33], the second term in Eq. (4a) is responsible for the thermal creep effect, which can cause velocity slip along the wall due to a temperature gradient adjacent to the wall along the surface. Even for a uniform wall temperature, $\partial T/\partial s$ at the wall is not identically zero. Yet, it can be shown through dimensional analysis that this term becomes second order in Knudsen number; thus, it can be neglected in the slip flow regime if compare to the first term, which is of order Kn. The relative importance of the second term in Eq. (4b) representing viscous dissipation depends on the Eckert number (or Mach number squared), and it may be considered negligible for low Mach number flows, which is consistent with the incompressible flow assumption made here. Therefore, as a reasonable approximation, only the first terms in the slip/jump boundary conditions will be retained in the present work.

The Reynolds number, $Re=\rho U_i D_h/\mu$, is based on the uniform inlet velocity and the hydraulic diameter D_h. Since the density is constant, $U_m=U_i$ everywhere in the channel. The Knudsen number is based on the hydraulic diameter as $Kn=\lambda/D_h$. In the present study, the Prandtl number is set equal to 1, and the effects of variations in Reynolds number ($0.1\leqslant Re\leqslant 10$), and channel aspect ratio ($0\leqslant\alpha^*\leqslant 1$) in the slip-flow regime ($Kn\leqslant 0.1$) are studied on the slip-flow development and heat transfer. Correlations are also provided for the key engineering parameters: friction factor and the Nusselt number.

3. The numerical method

The governing equations are integrated over the corresponding control volumes upon transformation into a generalized non-orthogonal coordinate system. The principle of the numerical method is based upon the calculation of the velocity field from momentum equations using the existing or approximate pressure field. This velocity field does not necessarily satisfy the mass conservation equation, and thus a velocity correction is introduced. A velocity potential is assigned to the velocity correction according to the Hodge decomposition theorem, which states that any vector function can be decomposed into a divergence-free component and the gradient of a scalar potential. This is consistent with the fact that an intermediate velocity field obtained form the momentum equations using an existing pressure field carries the exact vorticity field, and therefore, the velocity correction comes from an irrotational field that can be described with a velocity potential. The continuity equation is

then transformed into a Poisson equation for the velocity potential, which is solved with a matrix-free and pre-conditioned version of GMRES (Wigton et al. [34]). This method is capable of enhancing the convergence rate of the Poisson solver as compared to the traditional successive-over-relaxation solvers. Finally the pressure correction is directly related to the velocity correction through the momentum equations. The numerical scheme was originally developed by Chorin [35], and improved further by Dwyer [36] and the present authors [37]. Further enhancement in convergence rate of the solution procedure is achieved by implementing a pressure correction based on the average velocity defect $\Delta u'$ at each cross section of the channel such that [38]:

$$\Delta u' = \overline{U} - U_i \tag{5}$$

where $\overline{U}$ is the average velocity at a given cross section and U_i is the average inlet velocity. Assuming that the local velocity defect is associated with a pressure defect, the following equation can be formed:

$$\rho \frac{\Delta u'}{\Delta t} = -\frac{\partial p'}{\partial x} \tag{6}$$

Thus, the pressure field is updated with the above correction, and then the momentum equations are solved again with the new pressure field. This procedure significantly improves the computational efficiency.

3.1. Grid independence and validation

The grid points are clustered near the channel walls and in the entrance region, where large gradients exist. The cross-sectional grid resolution is studied by performing computations at $Re = 10$ with $Kn = 0.1$ for flow in a rectangular duct of $\alpha^* = 0.5$. The effect of several different grid sizes on some key flow parameters are listed in Table 1. This table shows that any grid size beyond 41×41 provides satisfactory cross-sectional resolution. The effect of axial grid resolution on the numerical results are studied with the same flow field and a fixed cross-sectional grid of 51×51. As shown in Fig. 2, the last two grid systems produce a variation of less than one percent in all monitored parameters. Therefore, a minimum mesh size of $141 \times 51 \times 51$ (x, y, z) is used with grid expansion ratios of about 1.06, 1.1 and 1.1 in the x, y, and z directions, respectively. The grid points are adjusted in the y-direction when the aspect ratio is increased to 1 to maintain good resolution. Channel lengths are set to a value greater than the estimated entrance length of the flow to ensure that fully developed conditions are achieved at the exit. Since the entrance length is a function of Re, Kn, and geometry, the channel length has been adjusted according to the case under consideration.

Table 1
Effects of cross-sectional grid resolution

Grid	$(f\,Re)_{\mathrm{fd}}$	$U_{\max}/U_i$	Nu_{fd}
31×31	8.28	1.571	2.72
41×41	8.35	1.579	2.73
51×51	8.38	1.582	2.74
61×61	8.40	1.584	2.75

Extensive validation studies have been conducted for flow in rectangular ducts and between parallel plates. In Tables 2 and 3 fully developed values of friction factor and heat transfer rate for flow between parallel plates have been compared with available analytical solutions at different Re and Kn. Friction factors in Table 2 show good agreement with the analytical values, which vary with Kn according to $f\,Re = 24/(1 + 12Kn)$. The Nusselt numbers in Table 3 are obtained for $Kn = 0$ over a large Re range. Note that even for no-slip flows, analytical results for constant wall temperature are available only for the limiting cases of $Re \gg 1$ (Shah and London [39]) or $Re \ll 1$ (Pahor and Strnad [40]). Fig. 3 compares the axial variation of the apparent friction factor and heat transfer coefficient for constant heat flux at the wall with data available in the literature, which indicates excellent agreement. More case validations can be found

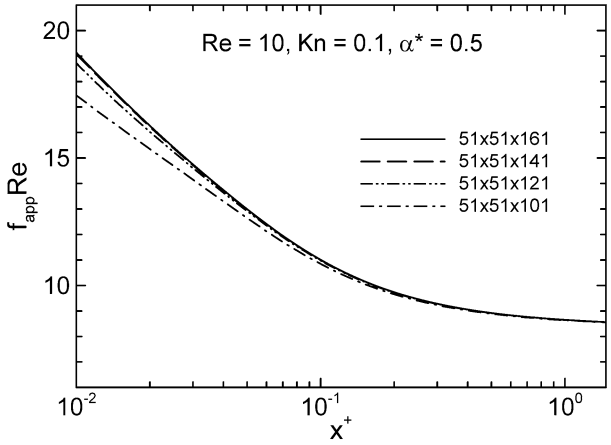

Fig. 2. Effect of axial grid distribution on the apparent friction coefficient.

Table 2
Friction factors for fully developed flow between parallel plates

Kn	$(f\,Re)_{\mathrm{fd}}$		
	Analytical solution	Present work	%
0	24.00	23.87	0.53
0.005	22.64	22.54	0.50
0.01	21.43	21.33	0.48
0.025	18.46	18.39	0.41
0.05	15.00	14.95	0.35
0.1	10.91	10.88	0.26

Table 3
Nusselt number for fully developed flow between parallel plates with constant wall temperature

Re	$(Nu)_{\mathrm{fd}}$	
	Present work	Analytical solution
0.1	8.105	8.093
1	8.000	
5	7.741	
10	7.624	
50	7.546	
100	7.542	7.543
500	7.541	7.540
1000	7.541	7.540

in Renksizbulut and Niazmand [37], Niazmand et al. [41], and Tercan [42].

As mentioned earlier, thermally developing flows in microchannels have been studied in the context of hydrodynamically fully developed flows, but it should be noted that the associated heat transfer rates in the thermally developing region are smaller than those in simultaneously developing flows. Such flows can be treated analytically when axial heat diffusion is neglected and a fully developed velocity profile is specified. However, the exclusion of the axial conduction is only valid for high Peclet number flows and therefore, limits the applicability of the results to gaseous microchannel flows. Yet, they can provide useful information for the accuracy of numerical studies. Yu and Ameel [24] solved the energy equation analytically for a constant wall temperature (neglecting axial conduction) by using a pre-specified slip velocity field. Fig. 4 shows a comparison of the axial variations of *Nu* for a thermally developing flow with the results of Yu and Ameel [24]. In the present solution, the numerically calculated fully developed velocity field with a specified slip at $Re = 200$ is fed into the energy equation to determine the temperature field in a rectangular channel ($\alpha^* = 0.5$) for different *Kn*. The comparison shows very good agreement for the slip-flow cases. The discrepancy observed for the no-slip case can be attributed to the exclusion of axial heat diffusion in their solution, considering the fact that axial conduction becomes more important as the rarefaction effects are reduced.

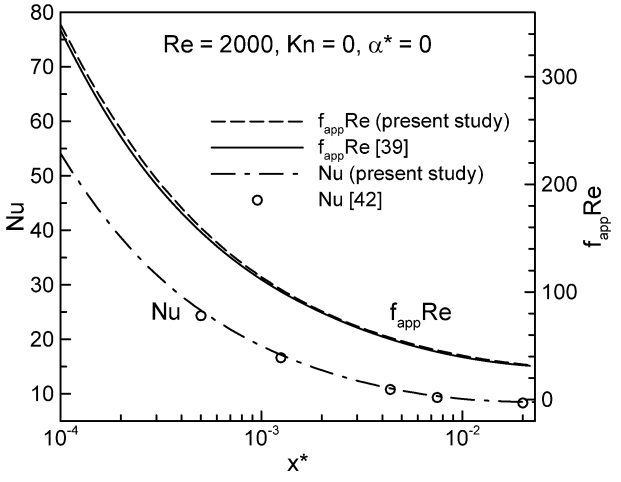

Fig. 3. Comparison of the axial variations of Nusselt number and apparent friction factor for constant heat flux at the wall.

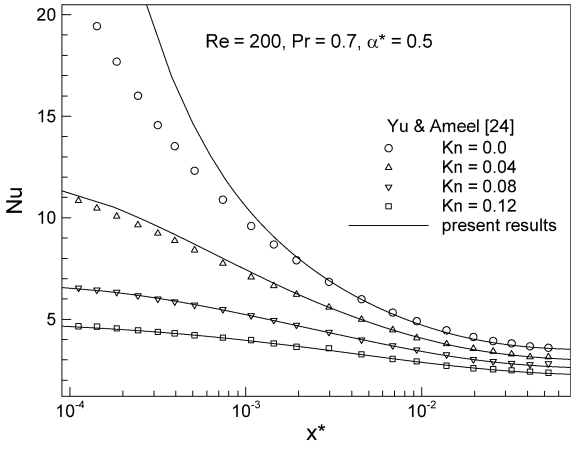

Fig. 4. Comparison of the axial variation of Nusselt number with the results of Yu and Ameel [24] at different *Kn*.

4. Results and discussion

4.1. The flow field

The global features of the flow development in the entrance region can be obtained by examining the velocity and pressure fields at different axial locations along the channel. In the fully developed region, non-axial velocity components are zero and pressure is uniform over a given cross section. However, in the entrance region, the flow is three-dimensional with a non-uniform pressure field at each cross section.

In Fig. 5, cross-sectional pressure distributions at two axial locations close to the inlet are shown for flow at $Re = 10$ in a square duct. For each cross-section, the dashed lines refer to the no-slip case, while the slip case for $Kn = 0.1$ is indicated by solid lines. These pressure contours clearly show the exis-

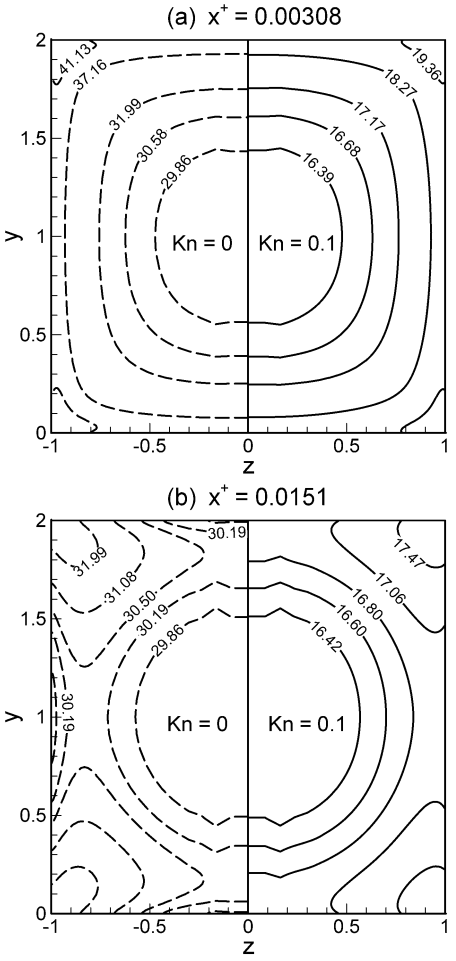

Fig. 5. Cross-sectional pressure distributions in a square duct at $Re = 10$: dashed lines $Kn = 0$, solid lines $Kn = 0.1$; (a) $x^+ = 0.00308$, (b) $x^+ = 0.0151$.

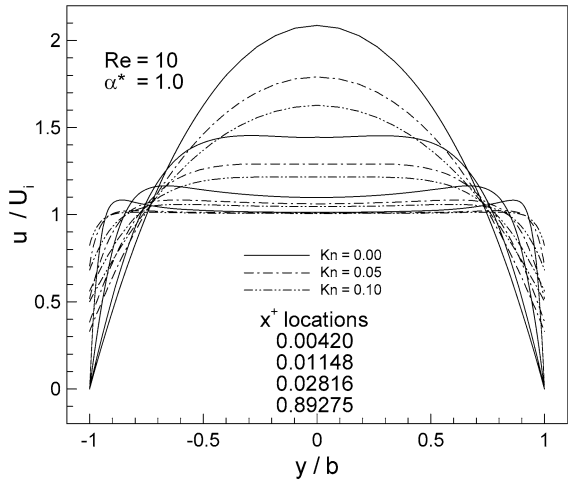

Fig. 6. Axial velocity profiles ($z = 0$ plane).

tence of local maxima near the walls, and in particular, in the corner regions of the channel. This is in fact due to the stagnation of the uniform inlet velocity at the walls for flows with $Kn < 0.001$ when the no-slip boundary condition is valid. As expected, slip at the wall reduces the pressure gradients in the cross section since the fluid particles are allowed to keep part of their inlet momentum at the wall depending on the Knudsen number. Strong pressure gradients that exist near the walls not only force the flow toward the core of the channel but also push the fluid near the walls in the axial direction. As shown in Fig. 6, this process causes the maximum velocities to be found near the walls rather than in the channel core as would normally be expected. This figure shows the stream-wise velocity profiles at four axial locations for a square duct at $Re = 10$ and three Knudsen numbers. Clearly, the amount of overshoot is directly related to the Knudsen number, which dictates the slip velocity at the wall. Allowing for slip reduces the amount of pressure generated as a result of the slowing down of the fluid particles at the wall. Even for high $Kn = 0.1$ there is still slight overshoots at the axial locations close to the inlet. Also, note that the amount of slip at a given Kn decreases as the flow approaches the fully developed region due to the reduction in the velocity gradients at the wall. Furthermore, higher slip is associated with the lower core velocities (as expected), and can be seen at all four axial locations.

In Figs. 7 and 8, three-dimensional velocity profiles at three axial locations are shown for flow in a square duct at $Re = 10$ for cases with $Kn = 0$ and $Kn = 0.1$, respectively. The axial locations of (a) $x^+ = 0.00308$ and (b) $x^+ = 0.0151$ are the same as those in Fig. 5 where the corresponding pressure distributions are presented. Flow is fully developed at the axial location of (c) $x^+ = 0.476$, and therefore, the pressure is uniform over the cross-section. The velocity contours in Figs. 7(a) and (b), show clearly that the highest axial velocities are located near the channel corners because the pressure gradients are the highest at these locations when no-slip boundary conditions are applied (see Fig. 5). Another feature of the velocity profiles in Figs. 7(a) and (b) is the presence of very large velocity gradients near the walls, resulting in correspondingly large friction coef-

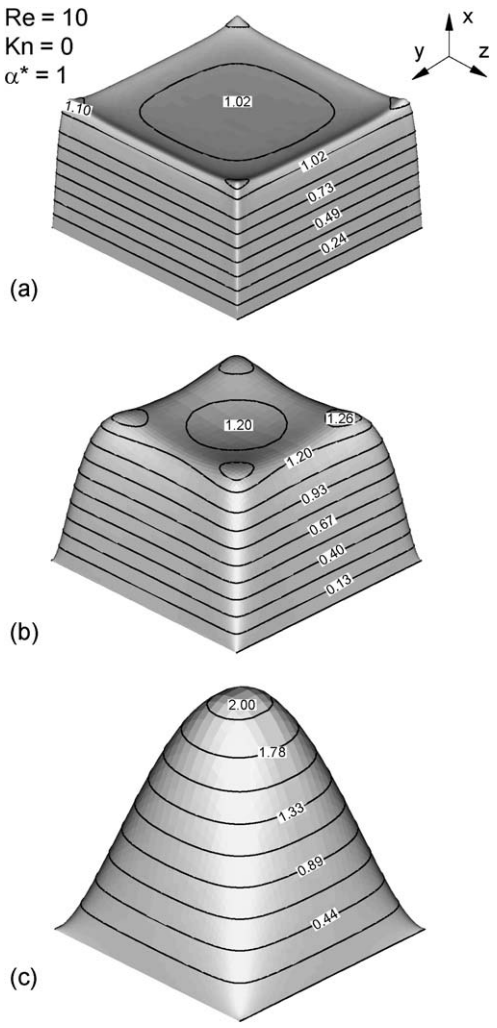

Fig. 7. Velocity profiles in a square channel at $Re = 10$ for $Kn = 0$: (a) $x^+ = 0.00308$, (b) $x^+ = 0.0151$, (c) $x^+ = 0.476$.

ficients early in the entrance region. Fig. (7c) shows the fully developed velocity profile where the low velocities and gradients inside the corners are noticeable features.

Figs. 8(a)–(c) show the corresponding velocity profiles for the case with $Kn = 0.1$. The prescribed uniform velocity profile at the inlet is only slightly affected in Fig. 8(a) due to the high velocity slip at the wall. The velocities in the corner regions are to some extent higher than the core for cross sections close to the inlet (Figs. 8(a) and (b)). It is also interesting to note that the minimum slip velocities occur at the corners at all axial locations because the velocity gradients normal to the wall are smaller in these regions. As indicated earlier in relation to Fig. 6, slip reduces the velocity gradients at the walls, and also reduces the extent of velocity overshoots. It is worth noting that such changes in axial velocity during the transformation from the uniform inlet profile to the fully developed state are more pronounced at higher Reynolds numbers (Niazmand et al. [41]). Channels with other aspect ratios develop similar flow patterns in the entrance region.

In the following, the effects of Re, Kn and α^* on the key engineering parameters (friction and heat transfer coefficients) are

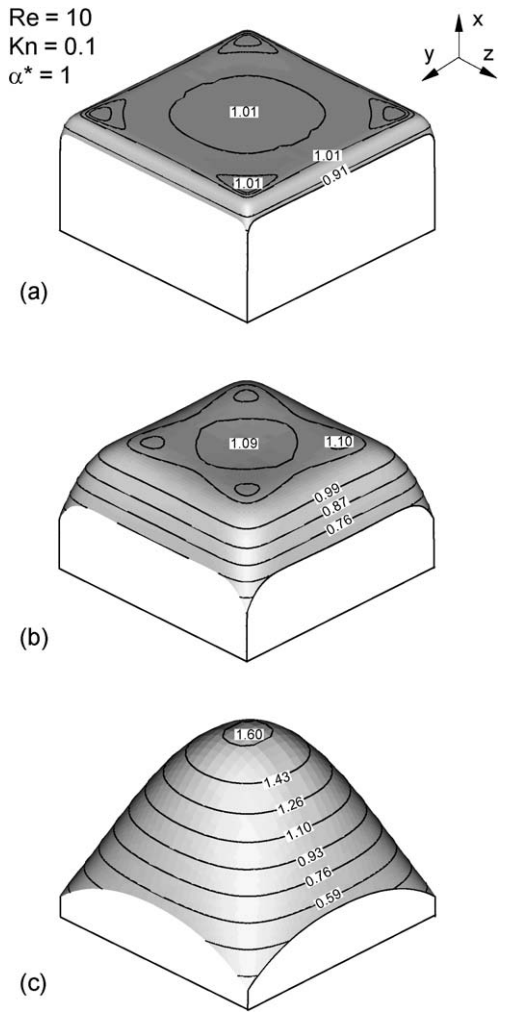

Fig. 8. Velocity profiles in a square channel at $Re = 10$ for $Kn = 0.1$: (a) $x^+ = 0.00308$, (b) $x^+ = 0.0151$, (c) $x^+ = 0.476$.

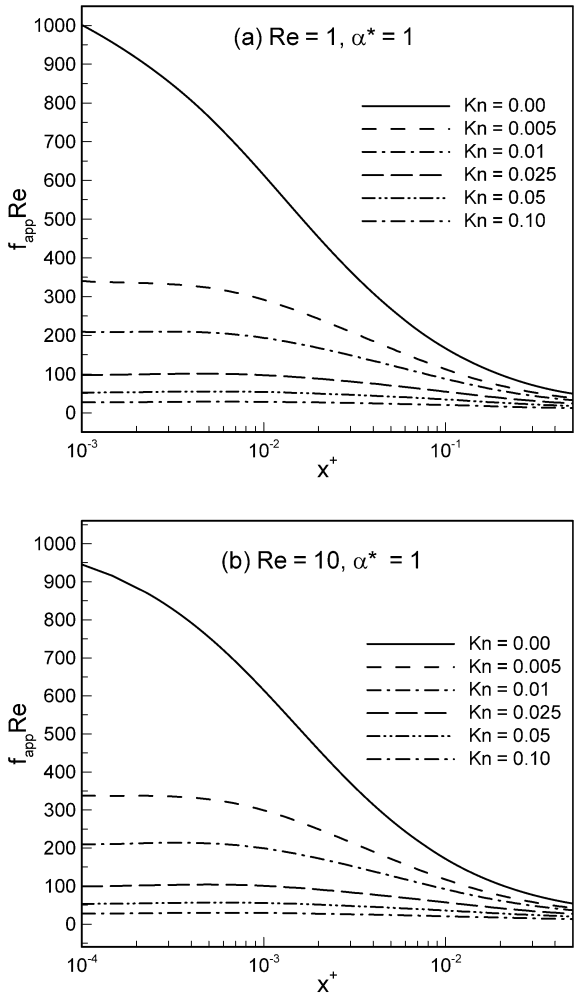

Fig. 9. Variation of apparent friction factor as function of Kn in a square duct: (a) $Re = 1$, (b) $Re = 10$.

discussed. The non-dimensional pressure drop along the channel is traditionally expressed in the form of an apparent Fanning friction factor defined as:

$$\frac{\Delta \bar{p}}{\rho U_i^2/2} = \frac{4x}{D_h} f_{\text{app}} = 4x^+ f_{\text{app}} Re = 4x^+ Po_{\text{app}} \tag{7}$$

where $\Delta \bar{p}$ indicates the pressure drop from the entrance, and $Po = f\,Re$ is the Poiseuille number.

In Figs. 9(a) and (b), the axial variations of $f_{\text{app}}Re$ are shown for a square duct as a function of Knudsen number at $Re = 1$ and 10, respectively. Unlike the fully developed region, where the pressure drop is only due to friction at the wall, in the developing region the change in the momentum rate accounts for a major part of the pressure drop. This figure clearly shows that in the entrance region, even small amounts of velocity slip results in a very large reduction in the friction coefficient. For a no-slip flow, $x^+ = 0$ is a singularity plane resulting in an infinitely large wall shear. On the other hand, for slip-flow, the asymptotic limit of the friction coefficient at the channel inlet is finite as seen in Figs. (9a) and (b), which can be obtained simply by substituting the velocity-slip boundary condition (Eq. (4a)) in the definition of the friction coefficient C_f. Thus, it can be easily shown that as $x^+ \to 0$: $f\,Re \to 2(2-\sigma_v)/(\sigma_v Kn)$. Interestingly, this asymptotic limit is valid for any geometry because it is only valid at a location where fluid is about to enter the channel, and therefore, there is no recognition of the geometry yet. Present numerical results provide data for $f_{\text{app}}Re$ at $x^+ > 0$ depending upon the grid spacing in the axial direction, but the extrapolated values are in good agreement with the expected asymptotic values.

The major drop in apparent friction coefficient at large Kn can also be justified based upon a comparison of the velocity profiles for $Kn = 0$ and $Kn = 0.1$ in Figs. 7 and 8, which indicates that secondary flows associated with the changes in the stream-wise velocity profile to reach to its final fully developed profile require much less momentum transfer for $Kn = 0.1$ and therefore, the corresponding $f_{\text{app}}Re$ drops dramatically as compared to the no-slip case. Similar behavior for $f_{\text{app}}Re$ at other Reynolds numbers, and in ducts with different aspect ratios, have been observed.

Fig. 10 shows the fully developed values of friction factor as a function of Kn for channels with different aspect ratios. At $Kn = 0$, the values of $f\,Re$ compare well with the results of Shah and London [39] at all aspect ratios. Furthermore, there is a good agreement with the results of Morini et al. [17], who

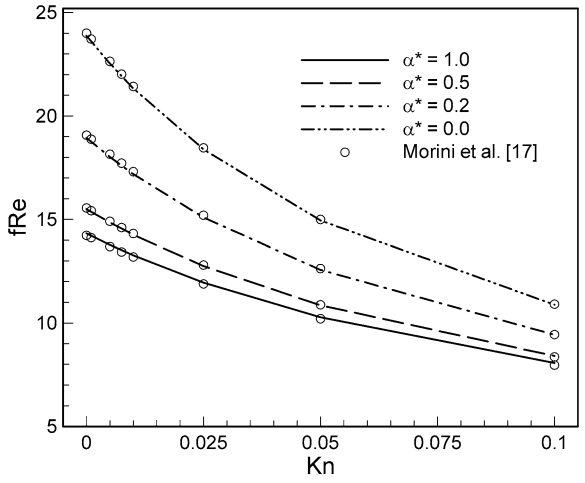

Fig. 10. Variation of fully-developed values of $f\,Re$ as a function of Kn and channel aspect ratio.

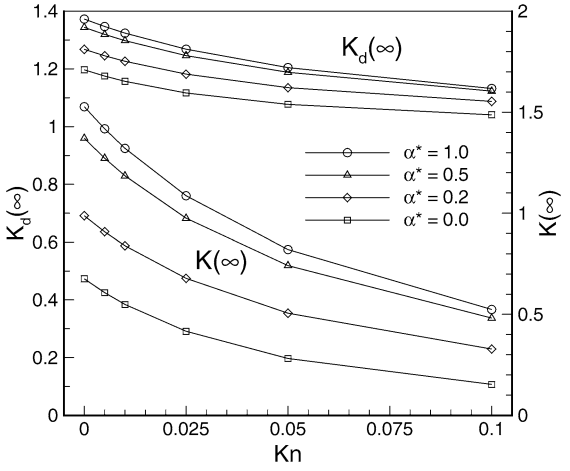

Fig. 11. Effects of Knudsen number on the momentum flux correction factor and the incremental pressure drop number for different α^* in the fully developed region.

have performed a 2-D analysis of fully developed flows for a wide range of aspect ratios and Kn. As expected, $f\,Re$ decreases monotonically with increasing Kn, which is about 42% at $Kn = 0.1$ for a square duct, while this value increases to about 53% for flow between parallel plates at the same Kn. Note that channel corners are regions of reduced slip due to weaker velocity gradients, and therefore, flow in a square duct is less sensitive to rarefaction effects than flow between parallel plates.

Two other fully developed parameters that are commonly reported are the momentum flux correction factor $K_d(x)$, and incremental pressure drop $K(\infty)$, as defined in [39]. In Fig. 11, both parameters are plotted as a function of Knudsen number for ducts with different aspect ratios. The values of the $K_d(x)$ and $K(\infty)$ for the no-slip cases compare well with the results in [39] for all aspect ratios. A monotonic decrease in both parameters are observed with increasing Kn, which is stronger for square ducts. The fact that both parameters are related to the fraction of the channel cross-section in which axial velocity is higher than the local mean velocity indicates that the wall dominated flows (square duct) have higher $K_d(x)$ and $K(\infty)$ than flat channels.

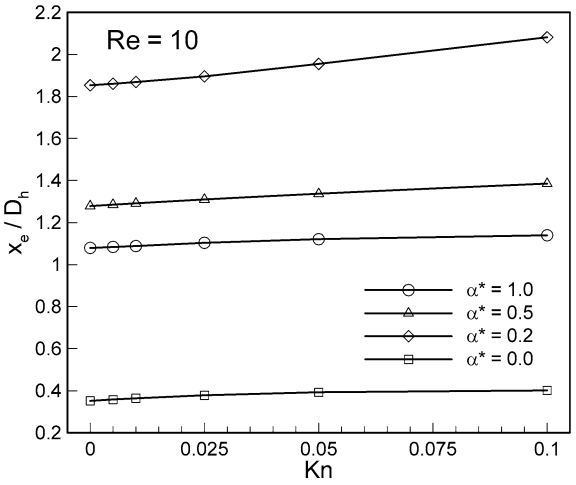

Fig. 12. Entrance lengths (x_e) for slip-flow at $Re = 10$ in rectangular channels with different aspect ratios.

The rarefaction effects on the entrance length are considered in Fig. 12. For a uniform inlet velocity profile, the entrance length is simply defined as the axial location where the maximum velocity attains 99% of its corresponding fully developed value. This figure shows the entrance lengths at various Kn and channel aspect ratios for $Re = 10$. Entrance lengths are observed to increase only marginally with the Knudsen number. Numerical results also indicate that this increase is slightly larger at higher Reynolds numbers. Note that entrance lengths display a highly non-linear dependence on the channel aspect ratio. Present results show that entrance lengths increase with increasing diffusion distance between the channel core and the corner regions. However, for very flat channels ($\alpha^* < 0.1$) the influence of the corners and sidewalls largely vanish. As such, flows between parallel plates have the shortest development lengths.

4.2. The temperature field

The temperature distribution at each cross section in the entrance region is affected by the geometry, Re, Pr and Kn numbers. Applying temperature-jump at the wall reduces the heat transfer rates, and therefore, lowers the fluid temperature as compared to no-slip/no-jump conditions. This effect is clear in Fig. 13, where the isotherms in a square duct at $Re = 10$ are shown at the same two axial locations corresponding to those in Fig. 5. Solid lines indicate the case with $Kn = 0.1$ while dashed lines refer to $Kn = 0$. Allowing for temperature-jump causes the fluid temperature adjacent to the wall to vary peripherally as indicated by solid lines in Fig. 13(b). The extent of temperature-jumps for this flow are clearly apparent in Fig. 14, where profiles in the plane of symmetry ($z = 0$) are shown. In this figure, three sets of temperature profiles corresponding to $Kn = 0, 0.05, 0.1$ at four axial locations are shown. Similar to the velocity profile, close to the inlet at $x^+ = 0.00202$, the temperature profile also shows strong gradients near the walls while the central region of the cross section is almost unaffected by the wall temperature. As expected, a very large temperature-jump occurs at this location due to the high temperature gradient near the wall for the $Kn = 0.05$ and 0.1 cases. Temperature

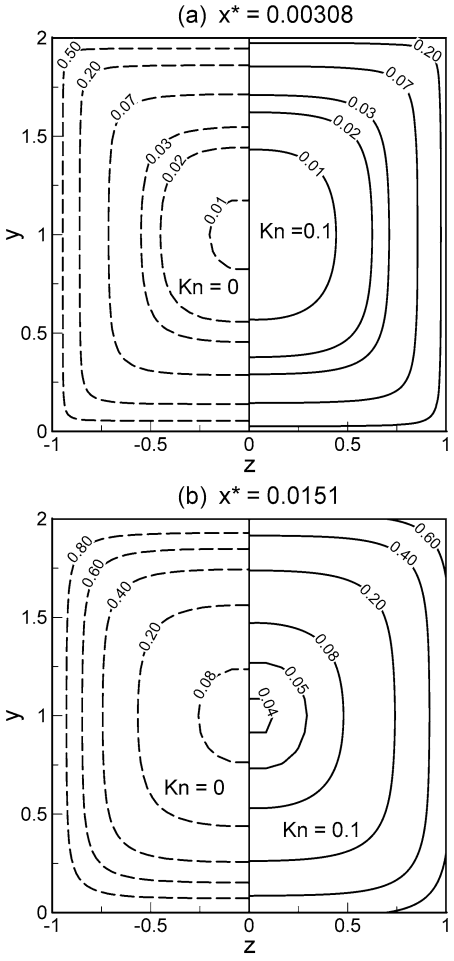

Fig. 13. Cross-sectional temperature distributions in a square duct at $Re = 10$: dashed lines $Kn = 0$, solid lines $Kn = 0.1$, (a) $x^* = 0.00308$, (b) $x^* = 0.0151$.

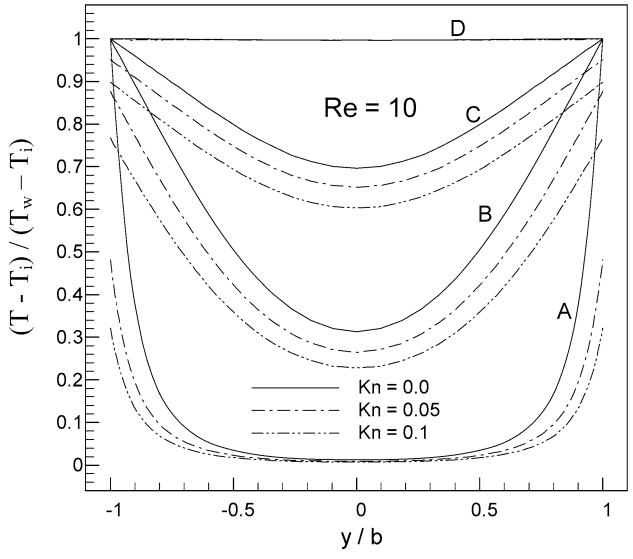

Fig. 14. Temperature profiles in a square duct at $Re = 10$ ($z = 0$ plane): (A) $x^* = 0.00202$, (B) $x^* = 0.0517$, (C) $x^* = 0.126$, (D) $x^* = 0.476$.

profiles at $x^+ = 0.0517$ (set B) indicate that the core region of the channel is now influenced by the constant wall temperature. It is clear that the temperature-jump at the wall for non-zero *Kn* cases reduces the amount of heat transfer from the wall.

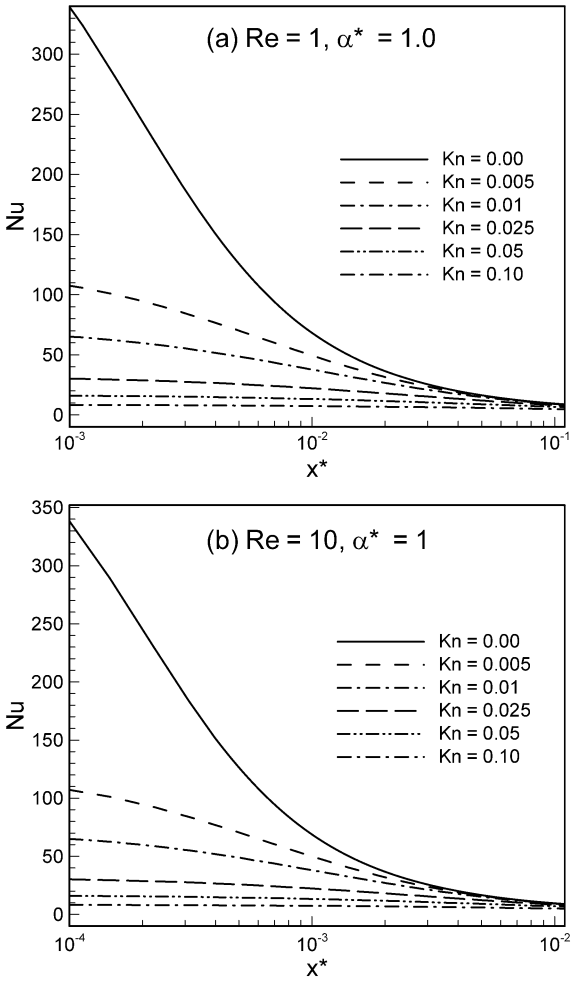

Fig. 15. Axial variation of Nusselt number in a square duct as a function of *Kn* for: (a) $Re = 1$, (b) $Re = 10$.

The variations in the heat transfer rate along the main flow direction for a square channel at several Knudsen numbers are shown in Figs. 15(a) and (b) for $Re = 1$ and 10, respectively. Despite the constant wall temperature, the heat transfer rate is neither peripherally nor axially constant in the entrance region even for the no-slip cases. The circumferentially averaged local heat transfer coefficient or the local Nusselt number is defined as:

$$Nu = \frac{h_x D_h}{k} = \frac{D_h(\overline{(\partial T/\partial n)_w})_x}{T_w - T_m} \tag{8}$$

where $\overline{(\partial T/\partial n)}_w$ is the peripherally-averaged temperature gradient normal to the wall at a given axial location, and $T_m(x)$ is the bulk mean temperature defined as:

$$T_m = \frac{1}{AU_i}\int_A T\vec{V}\cdot\vec{n}\,\mathrm{d}A \tag{9}$$

In the present work, $Pr = 1$ in all cases considered, and therefore, the non-dimensional axial length $x^* = x/(D_h Re\, Pr)$, or the reciprocal Graetz number, is the same as x^+ defined earlier.

Slip velocity by itself can increase heat transfer rate since it increases advection in a region where diffusion is dominant. However, the temperature-jump at the wall reduces the heat

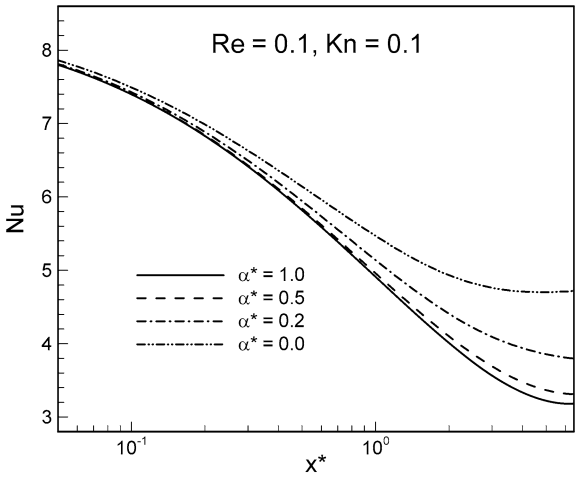

Fig. 16. Axial variation of Nusselt number at $Re = 0.1$ and $Kn = 0.1$ for different channel aspect ratios.

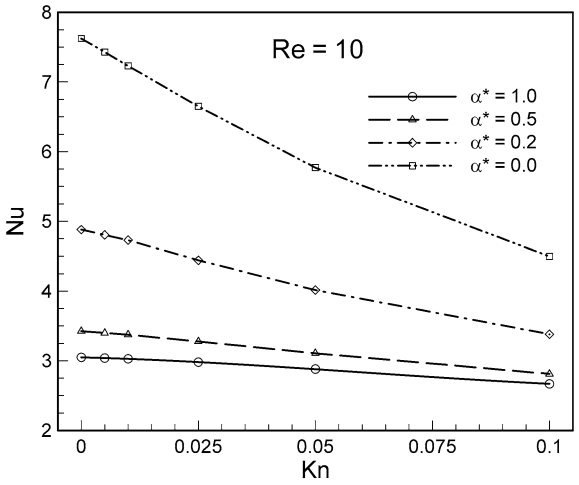

Fig. 17. Variation of fully developed *Nu* as a function of *Kn* and channel aspect ratio for flow at $Re = 10$.

transfer rate by creating an effect similar to contact resistance such that the net effect is a reduction in heat transfer. As shown in Fig. 15, velocity-slip together with temperature-jump dramatically reduces the heat transfer rates particularly early in the entrance region. A comparison between Figs. 15(a) and (b) indicates the existence of finite asymptotic values for *Nu* as $x^+ \to 0$ for slip-flows, which are not sensitive to the variation of *Re*. Using the definition of Nusselt number (Eq. (8)) together with the temperature-jump condition at the wall (Eq. (4b)), one can easily arrive at $Nu \to 1/C\,Kn$ as the asymptotic value for the inlet Nusselt number, where $C = [(2-\sigma_T)/\sigma_T][2\gamma/(\gamma+1)][1/Pr]$. Similar to the friction factor asymptotes given earlier, this value is independent of the *Re* and geometry since it is evaluated at a position where the flow still has no recognition of the geometry, and therefore, of the Reynolds number. Extrapolation of the present numerical results to $x^+ = 0$ compares well with this asymptotic *Nu* for the different cases studied here.

The fact that the inlet *Nu* is independent of the geometry can be also observed in Fig. 16 where the axial variation of the heat transfer coefficients are shown for different aspect ratios at $Kn = 0.1$ and $Re = 0.1$. For all α^*, the Nusselt number approaches a constant asymptotic value. Yet in the fully developed region, there is a clear distinction between different channels with the highest *Nu* for flow between parallel plates and the lowest for a square duct. It is also clear from Fig. 17, which shows the variation of the fully developed *Nu* as a function of *Kn* for different aspect ratios at $Re = 10$, that as the aspect ratio decreases towards the parallel-plates limit, stronger dependence on the *Kn* is observed. At this limit, there is about 40% decrease in *Nu* at $Kn = 0.1$ as compared to the no-slip case, while this value is much less (about 12%) for a square duct at the same condition. This effect can be explained considering the fact that for the parallel plates, the wall effect is peripherally uniform; that is at a given axial location along the channel, the velocity and temperature gradients at the wall are uniform around the duct, and therefore, the slip/jump effects are peripherally uniform. At the other extreme, for a square channel, there is a strong non-uniformity around the periphery with the corner regions behaving closer to the no-slip/no-jump conditions due to much lower velocity and temperature gradients there, and therefore, the *Kn* effects are overall weaker. This figure shows clearly that corner dominated flows are less sensitive to rarefaction effects.

5. Correlations

Friction factor and Nusselt number correlations previously developed by Renksizbulut and Niazmand [37] for no-slip flows in rectangular and trapezoidal channels (with acute side-angle ϕ) have been modified for rarefaction effects as given below:

$$(f\,Re)_{\rm fd} = \left[13.9\left(\frac{90^\circ}{\phi}\right)^{-0.07} + 10.4\exp\left(-3.25\alpha^*\left(\frac{90^\circ}{\phi}\right)^{0.23}\right)\right]G_1 \tag{10a}$$

$$G_1 = 1 - 2.48Kn^{0.64}\left(1 - 0.2\tanh(3\alpha^*)\right) \tag{10b}$$

$$(Nu)_{\rm fd} = \left[2.87\left(\frac{90^\circ}{\phi}\right)^{-0.26} + 4.8\exp\left(-3.9\alpha^*\left(\frac{90^\circ}{\phi}\right)^{0.21}\right)\right]G_2G_3 \tag{11a}$$

$$G_2 = 1 + 0.075(1+\alpha^*)\exp(-0.45Re) \tag{11b}$$

$$G_3 = 1 - 1.75Kn^{0.64}\left(1 - 0.72\tanh(2\alpha^*)\right) \tag{11c}$$

Although the present work is on rectangular microchannels only, the results of Morini et al. [17] have been used to evaluate the level of accuracy of the $(f\,Re)_{\rm fd}$ predictions for slip-flow in trapezoidal microchannels as well. Present numerical results for the friction coefficient are predicted within 6% with Eq. (10), while the results of Morini et al. [17] for rectangular ducts are predicted within 5% as shown in Fig. 18. However, the $(f\,Re)_{\rm fd}$ results for trapezoidal microchannels, which are only available for a side angle of $\phi = 54.74^\circ$, are estimated within 6%.

Eq. (11) predicts the present numerical heat transfer coefficients within 7% for all aspect ratios studied here, as shown

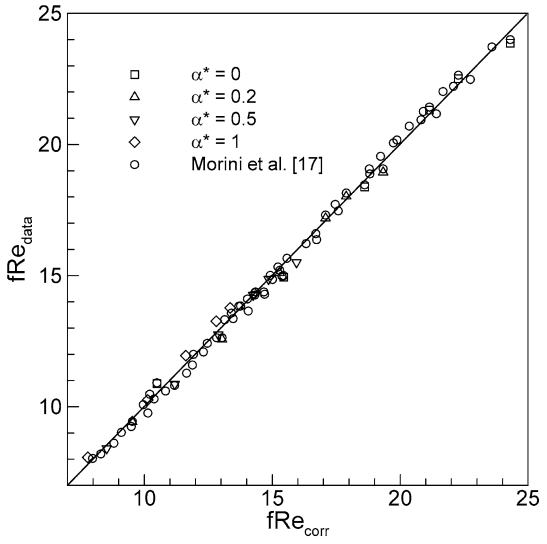

Fig. 18. Comparison of available data with the proposed friction coefficient correlation.

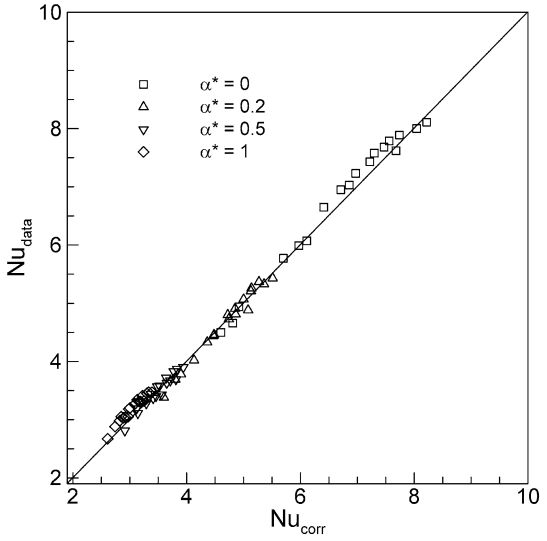

Fig. 19. Comparison of available data with the proposed heat transfer correlation.

in Fig. 19. Note that the Reynolds number dependence is more pronounced at low *Re* where axial conduction in the fluid cannot be ignored. Clearly, flows in microchannels with gas working fluids ($Pr \approx 1$) are low Peclet number flows, and correction for *Re* becomes important. Pahor and Strnad [40] showed a difference of about 10% in *Nu* between low and high *Pe* flows between parallel plates. While the proposed correlations are reasonably accurate, there is clearly a need for additional data on slip-flow in trapezoidal microchannels with different side angles.

6. Conclusions

The effects of rarefaction have been examined for simultaneously developing 3-D laminar, constant-property flows in rectangular microchannels for $Kn \leqslant 0.1$. Different channel aspect ratios ($0 \leqslant \alpha^* \leqslant 1$) were considered for Reynolds numbers in the range of $0.1 \leqslant Re \leqslant 10$ with $Pr = 1$. One of the interesting features of the flow development from a prescribed uniform profile at the inlet is the emergence of velocity over-shoots such that maximum axial velocities appear near the walls and especially at the corners as opposed to the channel core. This effect is more pronounced in the continuum regime ($Kn < 0.001$), yet it is still present to a lesser extent even at the higher end of the slip-flow regime at higher *Re*.

Due to the existence of large gradients near the channel entrance, velocity-slip and temperature-jump are both very large in this region. However, slip velocities are significantly reduced in the corner regions as the flow develops along the channel due to weaker velocity gradients. For the range of *Re* considered in the present study, entrance lengths are only marginally influenced by rarefaction effects, but they display a highly nonlinear dependence on the channel aspect ratios. The slip-flow regime is associated with very large reductions in wall friction and heat transfer in the entrance region as compared to the no-slip cases. In the fully developed region, both parameters are also significantly affected by the degree of rarefaction and the aspect ratio. They show a monotonic decrease with increasing *Kn*, and from the parallel-plates limit to the square-channel geometry. Fully developed values of friction coefficient and heat transfer rates are more influenced with rarefaction effects in a flat channel than a square duct due to the major influence of channel corners where rarefaction effects largely vanish. Practical engineering correlations are also provided for the friction and heat transfer coefficients in rectangular and trapezoidal channels.

Acknowledgement

Financial support from the Natural Sciences and Engineering Research Council of Canada is greatly appreciated.

References

[1] R. Edwards, Low density flows through tubes and nozzles, in: J. Potter (Ed.), Rarefied Gas Dynamics, AIAA, New York, 1977.
[2] P. Wu, W.A. Little, Measurements of friction factors for the flow of gases in very fine channels used for micro miniature Joule–Thomson refrigerators, Cryogenics 23 (1983) 273–277.
[3] J. Pfahler, J. Harley, H. Bau, J.N. Zemel, Gas and liquid flow in small channels, in: Proceedings of ASME Winter Annual Meeting, Micro Mechanical Sensors, Actuators, and Systems, DSC-32, ASME, New York, 1991, pp. 49–60.
[4] A. Beskok, G.E. Karniadakis, Simulation of slip-flows in complex microgeometries, J. Micromech. Syst. DSC 40 (1992) 355–370.
[5] E.B. Arkilic, K.S. Breuer, M.A. Schmidt, Gaseous flow in microchannels, in: Application of Microfabrication to Fluid Mechanics, ASME FED 197 (1994) 57–66.
[6] E.B. Arkilic, M.A. Schmidt, K.S. Breuer, Gaseous slip flow in long microchannels, J. Microelectromech. Syst. 6 (2) (1997) 167–178.
[7] J.C. Harley, Y. Huand, H. Bau, J.N. Zemel, Gas flow in microchannels, J. Fluid Mech. 284 (1995) 257–274.
[8] G.L. Morini, M. Spiga, Slip flow in rectangular microtubes, Microscale Thermophys. Engrg. 2 (1998) 273–282.
[9] A. Beskok, A model for flows in channels, pipes, and ducts at micro and nano-scales, Microscale Thermophys. Engrg. 3 (1999) 43–77.
[10] C.D. Meinhart, S.T. Wereley, J.G. Santiago, PIV measurements of a microchannel flow, Experiments in Fluids 27 (1999) 414–419.

[11] J. Jang, S.T. Wereley, Pressure distribution of gaseous slip flow in straight and uniform rectangular microchannels, Microfluid Nanofluid 1 (2004) 41–51.
[12] H. Xue, Q. Fan, A new analytic solution of the Navier–Stokes equations for microchannel flows, Microscale Thermophys. Engrg. 4 (2000) 125–143.
[13] T. Araki, M.S. Kim, H. Iwai, K. Suzuki, An experimental investigation of gaseous flow characteristics in microchannels, Microscale Thermophys. Engrg. 6 (2002) 117–130.
[14] S.S. Hsieh, H.H. Tsai, C.Y. Lin, C.F. Huang, C.M. Chien, Gas flow in a long microchannel, Int. J. Heat Mass Transfer 47 (2004) 3877–3887.
[15] S.E. Turner, L.C. Lam, M. Faghri, O.J. Gregory, Experimental investigation of gas flow in microchannels, J. Heat Transfer 126 (2004) 753–763.
[16] S. Colin, Rarefaction and compressibility effects on steady or transient gas flows in microchannels, in: Second International Conference on Microchannels and Minichannels, June 17–19, Rochester, New York, USA, 2004, pp. 13–24.
[17] G.L. Morini, M. Spiga, P. Tartarini, The rarefaction effects on the friction factor of gas flow in microchannels, Superlattices Microstruct. 35 (2004) 587–599.
[18] R.M. Inman, Laminar slip flow heat transfer in a parallel plate channel or a tube with uniform wall heating, NASA Report D-2393, 1964.
[19] R.F. Barron, X. Wang, R.O. Warrington, T.A. Ameel, Evaluation of the eigenvalues for the Graetz problem in slip-flow, Int. Commun. Heat Mass Transfer 23 (4) (1996) 563–574.
[20] R.F. Barron, X. Wang, T.A. Ameel, R.O. Warrington, The Graetz problem extended to slip-flow, Int. J. Heat Mass Transfer 40 (8) (1997) 1817–1823.
[21] H.P. Kavehpour, M. Faghri, Y. Asako, Effects of compressibility and rarefaction on gaseous flows in microchannels, Numer. Heat Transfer Part A 32 (1997) 677–696.
[22] T.A. Ameel, R.F. Barron, X. Wang, R.O. Warrington, Laminar forced convection in a circular tube with constant heat flux and slip flow, Microscale Thermophys. Engrg. 1 (4) (1977) 303–320.
[23] F.E. Larrodé, C. Housiadas, Y. Drossinos, Slip-flow heat transfer in circular tubes, Int. J. Heat Mass Transfer 43 (2000) 2669–2680.
[24] S. Yu, T.A. Ameel, Slip flow heat in rectangular microchannels, Int. J. Heat Mass Transfer 44 (2001) 4225–4234.
[25] S. Yu, T.A. Ameel, Slip-flow convection in isoflux rectangular microchannels, J. Heat Transfer 124 (2002) 346–355.
[26] G. Tunc, Y. Bayazitoglu, Heat transfer in rectangular microchannels, Int. J. Heat Mass Transfer 45 (2002) 765–773.
[27] N.G. Hadjiconstantinou, O. Simek, Constant-wall-temperature Nusselt number in micro and nano-channels, J. Heat Transfer 124 (2002) 356–364.
[28] Y. Asako, Heat transfer characteristics of gaseous flow in a micro-tube, in: Second International Conference on Microchannels and Minichannels, June 17–19, Rochester, New York, USA, 2004, pp. 305–311.
[29] J.C. Maxwell, On stresses in rarefied gases arising from inequalities of temperature, Philos. Trans. Roy. Soc. Part 1 170 (1879) 231–256.
[30] M. von Smoluchowski, Über wärmeleitung in verdünnten gasen, Ann. Phys. Chem. 64 (1898) 101–130.
[31] A. Beskok, G.E. Karniadakis, Simulation of heat and momentum transfer in complex micro-geometries, J. Thermophys. Heat Transfer 8 (1994) 647–653.
[32] C. Cercignani, The Boltzmann Equation and Its Applications, Springer, New York, 1988.
[33] E.H. Kennard, Kinetic Theory of Gases, McGraw-Hill, New York, 1939.
[34] L.B. Wigton, N.J. Yu, D.P. Young, GMRES acceleration of computational fluid dynamics codes, in: AIAA Computational Fluid Dynamics Meeting, Cinn., Ohio, 1985, pp. 67–74.
[35] A.J. Chorin, Numerical solution of the Navier–Stokes equations, Math. Comp. 22 (1968) 745–762.
[36] H.A. Dwyer, Calculation of droplet dynamics in high temperature environments, Prog. Energy Combust. Sci. 15 (1989) 131–158.
[37] M. Renksizbulut, H. Niazmand, Laminar flow and heat transfer in the entrance region of trapezoidal channels with constant wall temperature, J. Heat Transfer 128 (2006) 63–74.
[38] H.A. Dwyer, A.Y. Cheer, T. Rutaganira, N. Shacheraghi, Calculation of unsteady flows in curved pipes, J. Fluids Engrg. 123 (2001) 869–877.
[39] R.K. Shah, A.L. London, Laminar Flow Forced Convection in Ducts, Advances in Heat Transfer, Academic Press, New York, 1978.
[40] S. Pahor, J. Strnad, A note on heat transfer in laminar flow through a gap, Appl. Sci. Res. Sect. A 10 (1961) 81–84.
[41] H. Niazmand, G. Tercan, M. Renksizbulut, Entrance region flows in rectangular microchannels with constant wall temperature, in: Proceedings of ICMM2005, 3rd International Conference on Microchannels and Minichannels, June 13–15, 2005, Toronto, Canada.
[42] G. Tercan, Heat transfer and fluid flow in rectangular microchannels, MSc Thesis, University of Waterloo, Waterloo, Ontario, Canada, 2005.